# Photoacoustic-Imaging-Based Temperature Monitoring for High-Intensity Focused Ultrasound Therapy

Xun Wu, Jean Lunsford Sanders, Douglas N. Stephens, *Member, IEEE*, and Ömer Oralkan, *Senior Member, IEEE*

***Abstract*—Temperature monitoring during high-intensity focused ultrasound (HIFU) application is necessary to ensure effective therapy while minimizing thermal damage to adjacent tissue. In this study, we demonstrate a noninvasive approach for temperature measurement during HIFU therapy based on photoacoustic imaging (PAI). Because of the dependence of photoacoustic (PA) signal amplitude on temperature of the source tissue and the linearity of the PAI system, changes in temperature will cause changes in PA image intensity. Experiments have been conducted in *ex-vivo* bovine tissue to characterize the linear dependence of PA image pixel values on temperature and subsequently to convert the PA image to a real-time temperature map.**

## I. Introduction

It is necessary to monitor the temperature distribution during HIFU therapy to ensure effective destruction of target tissue and minimize thermal damage to the surrounding healthy tissue. A thermocouple or a fluoroptic temperature sensor can be used to measure temperature accurately in tissue, but this approach is invasive and cannot monitor temperature distribution in a wide area. Magnetic resonance imaging (MRI) provides a noninvasive way to monitor temperature distribution with high accuracy [1], but it is bulky, slow, and expensive [2]. Ultrasound (US) imaging-based methods provide a portable, real-time, and low-cost alternative but with limited accuracy due to the weak temperature sensitivity [3], [4]. Optical methods that are portable and sensitive have been developed [5]. However, their penetration depth is limited due to the strong scattering of light inside tissue.

PAI is an emerging hybrid imaging modality that combines the contrast of optical absorption with the deep penetration depth and high spatial resolution of US imaging [6]. It is particularly appealing for noninvasive temperature monitoring during HIFU therapy because of the PA signal's high sensitivity to temperature [7], its high compatibility with HIFU, and real-time capability. In this paper, we develop a temperature measurement approach based on PAI. PA image pixel values are used to calculate the temperature at each pixel location based on the dependence of PA signal intensity on temperature. Experiments have been performed on bovine tissue samples. Earlier work on using PA effect for temperature measurement has been primarily based on using single-element transducers and analysis of the amplitude of the PA RF A-scan data [7-9]. In the present work, we extend this approach to the use of full-field PA images and demonstrate the calculation of a real-time temperature map once the Grüneisen coefficient's dependence on temperature is known.

The presented work is part of our greater effort aiming to implement a minimally invasive triple-modality instrument that combines 3D US imaging, HIFU, and PAI capabilities for navigation, ablative therapy, and lesion monitoring, respectively [10].

The following section presents a theoretical background for the developed temperature monitoring approach. Experimental methods are described next, followed by the presentation of the results and related discussion.

## II. Theoretical Background

### A. Linear Dependence of the PA Signal Amplitude on Temperature

The PA effect is the physical basis for PAI. It refers to the generation of acoustic waves introduced by the absorption of electromagnetic energy. The thermal expansion of tissue caused by a short laser pulse induces a pressure rise $P$, which can be calculated as [7]:

$$P = \mu_a \Gamma(T) F, \tag{1}$$

where $F$ is the laser fluence, $\mu_a$ is the absorption coefficient of the tissue, and $\Gamma(T)$ is the temperature-dependent Grüneisen parameter:

$$\Gamma(T) = A+BT, \tag{2}$$

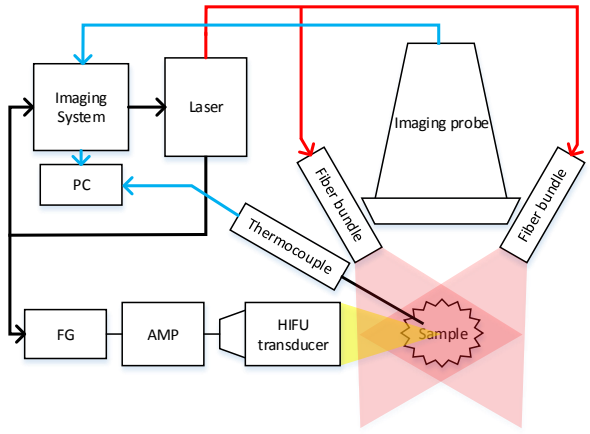


Fig. 1. Experimental setup. FG: function generator; AMP: power amplifier.

This work is supported by the National Institutes of Health (NIH) under grant 1R01HL117740.

X. Wu, J. L. Sanders, and Ö. Oralkan are with the Department of Electrical and Computer Engineering, North Carolina State University, Raleigh, NC 27695 USA (e-mail: xwu12, jelunsfo, ooralka@ncsu.edu).

D. N. Stephens is with the Department of Biomedical Engineering, University of California, Davis, CA 95616 USA (e-mail: dnstephens@ucdavis.edu).

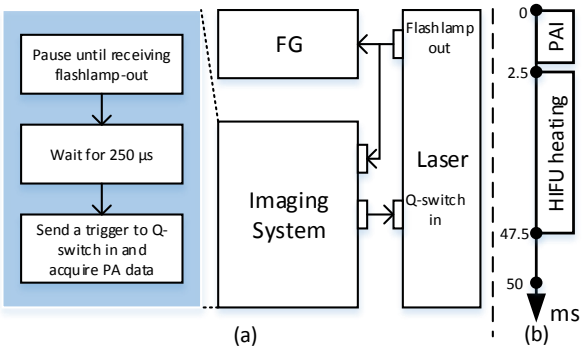


Fig. 2. (a) Triggering scheme. (b) Timing diagram.

where $A$ and $B$ are constants that depend on tissue properties and $T$ is the temperature. Combining (1) and (2):

$$P = C+DT, \tag{3}$$

where C = $\mu_a FA$ and D = $\mu_a FB$, thus the pressure of the PA signal generated due to PA effect can be used to monitor the temperature as long as $C$ and $D$ are calibrated properly.

### B. Linearity of the PAI System

The PAI system is a linear system. Ideally, the pixel values in a PA image linearly scale with the pressure rise caused by the PA effect and thus the value of a pixel $V(x,y)$ in a PA image is proportional to the pressure rise at the corresponding location in the imaging field:

$$V(x,y) = EP(x,y) + N \tag{4}$$

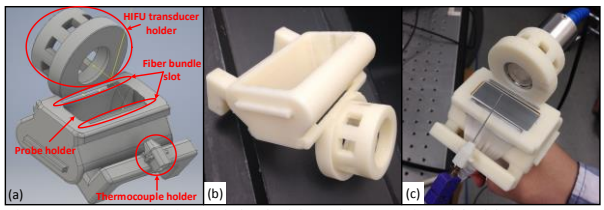


Fig. 3. (a) CAD design of the holder. (b) 3D printed holder. (c) HIFU transducer, imaging probe and the hypodermic thermocouple probe in place.

Combining (3) and (4)

$$V(x,y) = G + HT(x,y) + N, \tag{5}$$

where $G = \mu_a(x,y)F(x,y)AE$, $H = \mu_a(x,y)F(x,y)BE$, E is a constant that depends on the PAI system, and N is the system's added noise. So, we can monitor the temperature in the imaging field of PA images with their pixel values as long as G and H are known beforehand.

## III. Methods

### A. Experimental Setup

Fig. 1 shows a block diagram of the experimental setup. A tunable laser system (Model Phocus Mobile, Opotek Inc., Carlsbad, CA) with a customized dual-output fiber is used for PAI. The laser is set to work at 710-nm wavelength with a 20-Hz repetition rate. The width of the laser pulse is 5 ns and the energy per pulse is 5 mJ at the output of the dual-output fiber, which has a 40-mm by 0.25-mm aperture size on each

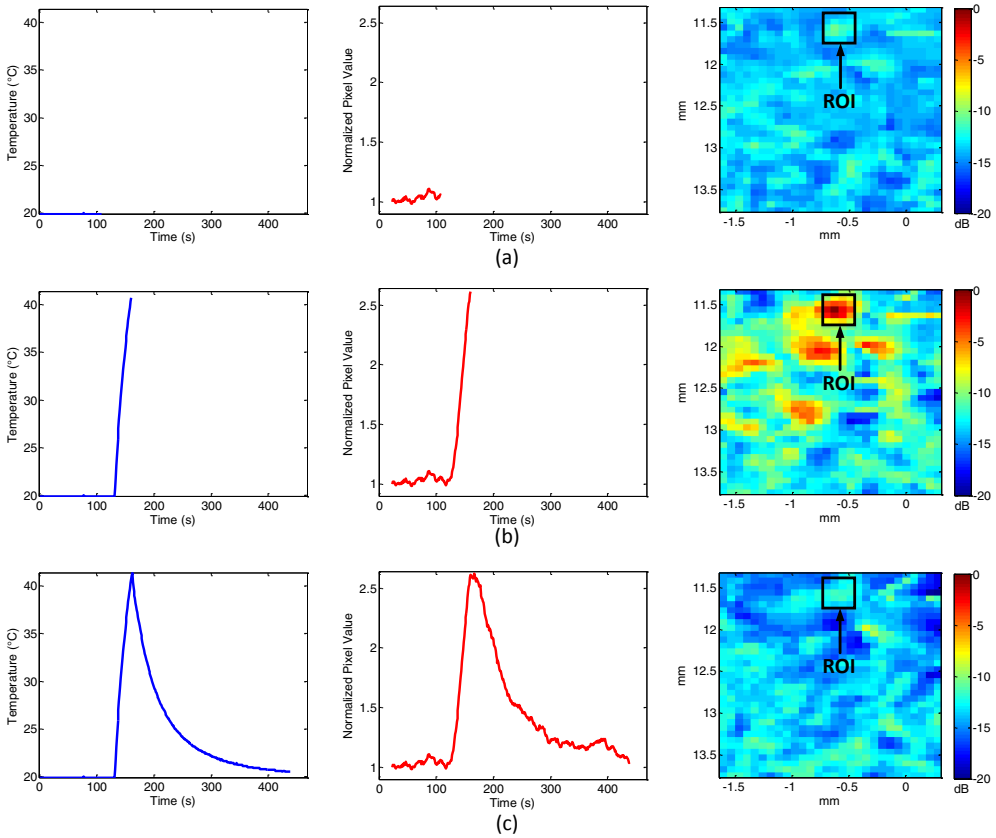


Fig. 4. Left column shows temperature recorded by the thermocouple as a function of time; Middle column shows normalized average pixel intensity in the ROI as a function of time; Right column shows the reconstructed PAIs normalized to the first frame in the sequence at (a) 108 seconds, (b) 160 seconds, (c) 438 seconds.

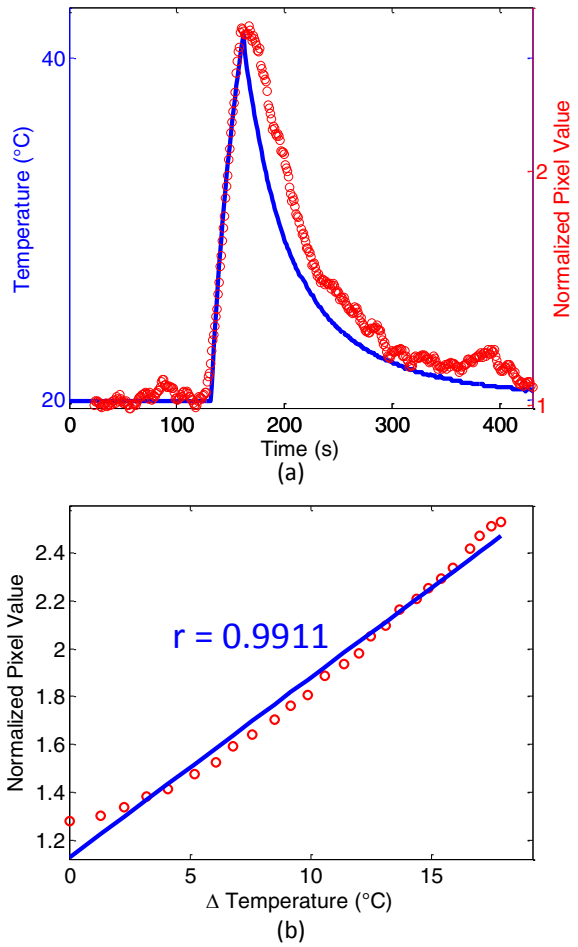


Fig. 5. (a) Recorded temperature and normalized average pixel value in the ROI as a function of time. (b) Normalized average pixel value in the ROI as a function of change in temperature.

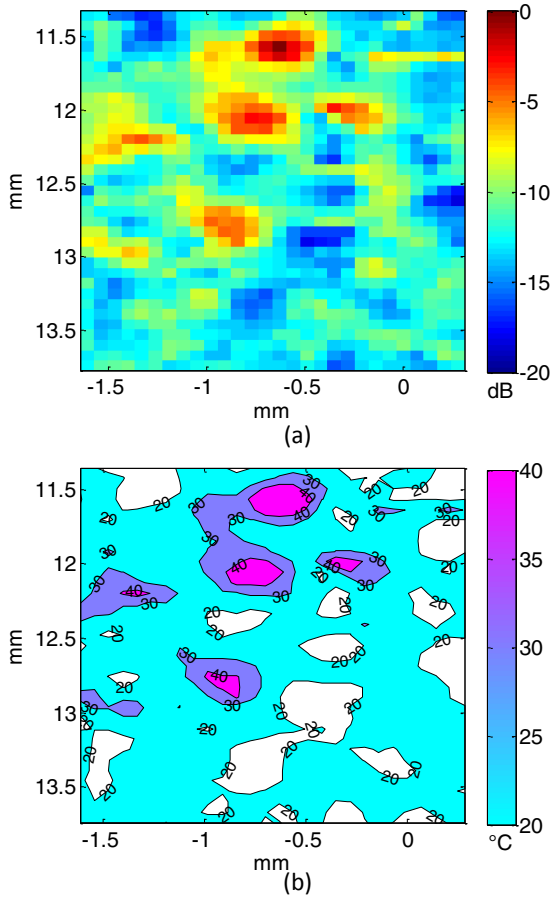


Fig. 6. (a) PA image near the ROI. (b) Calculated temperature map near the ROI with isothermal regions bounded by contours.

branch. The flash lamp trigger output signal of the laser serves as the master clock that drives the system. A programmable imaging system (Model Vantage 64 LE, Verasonics, Inc., Kirkland, WA), a PC (Model Precision T5610, Dell Inc., Round Rock, TX), and a linear ultrasound transducer array (Model L7-4, Philips, Bothell, WA) are used for PA data acquisition. The programmable imaging system has 64 parallel receive channels with 2:1 multiplexing capability to receive from all of the 128 elements of the linear array. As a result, to receive the data to construct a complete frame, the laser has to fire twice. A function generator (Model 33500B, Agilent Technologies Inc., Santa Clara, CA) and an RF power amplifier (Model 210L, Electronics & Innovation, Ltd., Rochester, NY) are used to excite the HIFU transducer (5-MHz, 19-mm circular aperture, 15-mm focal distance, Precision Acoustics Ltd., Dorchester, Dorset, UK). The function generator is triggered by the flash lamp trigger output to generate a burst of 225,000 cycles of 5-MHz sinusoidal signal with a 2.5-ms delay after it is triggered. The 5-MHz, 450-mVpp sinusoidal signal is amplified by the RF power amplifier with a gain of 40 dB to reach an acoustic intensity of 5 kW/cm$^2$ at the HIFU focus. A hypodermic thermocouple probe (Model HYP5-21-1-1/2-E-G-SMPW-M, OMEGA Engineering, Inc., Stamford, CT) is used for acquisition of the temperature data at a rate of 1 sample/s.

The data acquisition process starts with the flash lamp firing at a 20-Hz repetition rate. The imaging system receives the trigger output signal from the flash lamp, waits for 250 µs and sends a trigger signal to the Q-switch trigger-in port of the laser. This signal triggers the Q-switch so that the laser fires and the imaging system starts acquiring PA data concurrently. This triggering scheme is shown in Fig. 2(a). HIFU application starts 2.5 ms after the PA data acquisition is initiated so that the HIFU heating and PA data acquisition processes are interleaved to eliminate the interference. A timing diagram of this process is shown in Fig. 2(b).

### *B. Component Coregistration*

A custom holder (Fig. 3) is designed in a 3D computer-aided design (CAD) environment (Autodesk Inventor, Autodesk, Inc., San Rafael, CA) to hold the ultrasound transducer array, dual-output laser fiber, HIFU transducer, and the thermocouple. It is designed in such a way that the focal point of the HIFU transducer, the laser illumination direction, and the tip of the thermocouple are overlapped on the imaging plane, as shown in Fig. 3(c).

### *C. Experimental Procedure*

Sample *ex-vivo* bovine tissue is cut into small cubes (approximately 1.5 cm × 1.5 cm × 1.5 cm) and attached to the

tip of the thermocouple. The PA data acquisition process is started after the thermocouple temperature logging is initiated. After capturing the baseline temperature for 2 minutes, HIFU is applied to heat the sample tissue for 30 seconds. After the HIFU heating process is completed, the system continues acquiring PA data for another approximately 5 minutes until the temperature read by the thermocouple returns to baseline.

### *D. Data Processing*

PA images are reconstructed from the acquired data using standard time-domain delay-and-sum beamforming. PA image frames are averaged and displayed at a rate of 1 fps. Normalization of the PA image frames to the initial frame acquired prior to heating helps minimize the image artifacts that could be caused by nonuniform optical fluence and nonuniform absorbance [11]. Assuming these are not temperature dependent factors, changes in the normalized images then can all be attributed to changes in the Grüneisen coefficient as a function of temperature. According to the calibration of the thermocouple tip position, a region of interest (ROI), which is a small area (approximately 0.4 mm × 0.4 mm) around the thermocouple tip, commensurate with the focal spot size of the HIFU transducer, is cropped in the PA images. The average pixel value is calculated for the ROI in each PA image and compared with the temperature data captured by the thermocouple.

Linear regression is used to extract and evaluate the linear relationship between the temperature and the normalized average pixel value, which is then used to calculate the temperature at each pixel in the PA image and generate a map that shows the temperature distribution in the field of PA images.

## IV. Results and Discussion

It is clearly seen in Fig. 4 (right column), that the PA image intensity near the HIFU focus increases as the temperature rises and decreases as the temperature returns to the baseline.

As mentioned in the theoretical background, the changes of PA image intensity at each pixel can be used to calculate the temperature change at that location if the relationship between PA image pixel value and the temperature is known.

For the acquired data set we analyzed the relationship between the average pixel value in the ROI and the recorded temperature (Fig. 5). Once we established this linear relationship we converted the acquired PA image to a temperature map (Fig. 6).

The presented results demonstrate high-precision and spatially high-resolution temperature mapping because of the precise temperature-to-image-intensity calibration based on thermocouple recordings in our experiments. Translation of the presented approach to *in-vivo* applications requires characterization of the Grüneisen parameter's temperature dependence for different tissue types. Even then, spatial variation and sample-to-sample difference could result in inaccuracies in the calculation of temperature maps. Recently it has been shown that imaging hemoglobin at its isosbestic point could serve as a universal photoacoustic sensor for noninvasive temperature monitoring in vascularized tissues independent of tissue composition [12], which increases the confidence in translating the approach presented in this paper to *in-vivo* applications for HIFU ablative therapies.

## V. Conclusion

We demonstrated the proof of principle for a noninvasive approach for temperature monitoring during HIFU therapy based on PAI. We showed that if, for a given tissue type, the temperature dependence of Grüneisen coefficient is known, a spatiotemporally high-resolution temperature map can be generated in real time to guide HIFU ablative therapies.


## Acknowledgment

The authors thank Steven Lucero for technical assistance in the 3D CAD modeling of the probe holder.


## References


[1] C. Mougenot *et al*., "Automatic spatial and temporal control for MR-guided focused ultrasound using fast 3D MR thermometry and multispiral trajectory of the focal point," *Magn. Reson. Med*., vol. 52, no. 5, pp. 1005–1015, Nov. 2004.

[2] P. Steiner *et al*., "Radio-frequency-induced thermoablation: monitoring with T1-weighted and proton-frequency-shift MR imaging in an interventional 0.5-T environment," *Radiology*, vol. 206, no. 3, pp. 803-810, Mar. 1998.

[3] R. Seip *et al*., "Noninvasive real-time multipoint temperature control for ultrasound phased array treatments," *IEEE Trans. Ultrason., Ferroelectr. Freq. Control.* vol. 43, no. 6, pp. 1063-1073, Nov. 1996.

[4] C. Simon *et al*., "Two-dimensional temperature estimation using diagnostic ultrasound," *IEEE Trans. Ultrason., Ferroelectr. Freq. Control*, vol. 43, no. 6, pp. 1088–1099, Jul. 1998.

[5] M. Bakhsheshi *et al*., "Monitoring brain temperature by time-resolved near-infrared spectroscopy: Pilot study," *J. Biomed. Opt*., vol. 19, no. 5, pp. 057005-1–057005-9, May 2014.

[6] L. Wang and H. Wu, "Biomedical Optics: Principles and Imaging," Hoboken, N.J.: Wiley-interscience, 2007.

[7] I. Larina, K. Larin and R. Esenaliev, "Real-time optoacoustic monitoring of temperature in tissues," *J. Phys. D: Appl. Phys*., vol. 38. No. 15, pp. 2633–2639, 2005.

[8] M. Pramanik and L. Wang, "Thermoacoustic and photoacoustic sensing of temperature," *J. Biomed. Opt.*, vol. 14, no. 5, pp. 054024-1-7, Sep/Oct 2009.

[9] F. Xiaohua, G. Fei, and Z. Yuanjin, "Photoacoustic-based-close-loop temperature control for nanoparticle hyperthermia," *IEEE Tran. Biomed. Eng.*, vol. 62, no. 7, pp. 1728-1737, Jul. 2015.

[10] J. H. Jang, M. F. Rasmussen, A. Bhuyan, H.-S. Yoon, A. Moini, C. Chang, R. D. Watkins, J. W. Choe, A. Nikoozadeh, D. Stephens, Ö. Oralkan, K. Butts-Pauly, and B. T. Khuri-Yakub, "Dual-mode integrated circuit for imaging and HIFU with 2-D CMUT arrays," *Proc. IEEE. Intl. Ultrason. Symp.*, pp. 1-4, 2015.

[11] E. V. Petrova, S. A. Ermilov, R. Su, V. V. Nadvoretsky, A. Conjusteau, and A. A. Oraevsky, "Temperature dependence of Grüneisen parameter in optically absorbing solutions measured by 2D optoacoustic imaging," in *Proc. SPIE*, vol. 8943, pp. 89430S-1-6, 2014.

[12] E. V. Petrova, A. A. Oraevsky, and S. A. Ermilov, "Red blood cell as a universal optoacoustic sensor for non-invasive temperature monitoring," *Appl. Phys. Lett.*, vol. 105, no. 9, pp. 094103, 2014.